



HAL
open science

Extreme secular excitation of eccentricity inside mean motion resonance

Gabriele Pichierri, Alessandro Morbidelli, Dong Lai

► **To cite this version:**

Gabriele Pichierri, Alessandro Morbidelli, Dong Lai. Extreme secular excitation of eccentricity inside mean motion resonance: Small bodies driven into star-grazing orbits by planetary perturbations. *Astronomy and Astrophysics - A&A*, 2017, 605, pp.A23. 10.1051/0004-6361/201730936 . hal-02959633

HAL Id: hal-02959633

<https://hal.science/hal-02959633>

Submitted on 6 Oct 2020

HAL is a multi-disciplinary open access archive for the deposit and dissemination of scientific research documents, whether they are published or not. The documents may come from teaching and research institutions in France or abroad, or from public or private research centers.

L'archive ouverte pluridisciplinaire **HAL**, est destinée au dépôt et à la diffusion de documents scientifiques de niveau recherche, publiés ou non, émanant des établissements d'enseignement et de recherche français ou étrangers, des laboratoires publics ou privés.

Extreme secular excitation of eccentricity inside mean motion resonance

Small bodies driven into star-grazing orbits by planetary perturbations^{*}

Gabriele Pichierri¹, Alessandro Morbidelli¹, and Dong Lai²

¹ Laboratoire Lagrange, Université Côte d'Azur, Observatoire de la Côte d'Azur, CNRS, CS 34229, 06304 Nice, France
e-mail: gabriele.pichierri@oca.eu

² Cornell Center for Astrophysics and Planetary Science, Department of Astronomy, Cornell University, Ithaca, NY 14853, USA

Received 4 April 2017 / Accepted 1 May 2017

ABSTRACT

Context. It is well known that asteroids and comets fall into the Sun. Metal pollution of white dwarfs and transient spectroscopic signatures of young stars like β -Pic provide growing evidence that extra solar planetesimals can attain extreme orbital eccentricities and fall into their parent stars.

Aims. We aim to develop a general, implementable, semi-analytical theory of secular eccentricity excitation of small bodies (planetesimals) in mean motion resonances with an eccentric planet valid for arbitrary values of the eccentricities and including the short-range force due to General Relativity.

Methods. Our semi-analytic model for the restricted planar three-body problem does not make use of series expansion and therefore is valid for any eccentricity value and semi-major axis ratio. The model is based on the application of the adiabatic principle, which is valid when the precession period of the longitude of pericentre of the planetesimal is much longer than the libration period in the mean motion resonance. In resonances of order larger than 1 this is true except for vanishingly small eccentricities. We provide prospective users with a Mathematica notebook with implementation of the model allowing direct use.

Results. We confirm that the 4:1 mean motion resonance with a moderately eccentric ($e' \lesssim 0.1$) planet is the most powerful one to lift the eccentricity of planetesimals from nearly circular orbits to star-grazing ones. However, if the planet is too eccentric, we find that this resonance is unable to pump the planetesimal's eccentricity to a very high value. The inclusion of the General Relativity effect imposes a condition on the mass of the planet to drive the planetesimals into star-grazing orbits. For a planetesimal at ~ 1 AU around a solar mass star (or white dwarf), we find a threshold planetary mass of about 17 Earth masses. We finally derive an analytical formula for this critical mass.

Conclusions. Planetesimals can easily fall into the central star even in the presence of a single moderately eccentric planet, but only from the vicinity of the 4:1 mean motion resonance. For sufficiently high planetary masses the General Relativity effect does not prevent the achievement of star-grazing orbits.

Key words. celestial mechanics – planets and satellites: dynamical evolution and stability – minor planets, asteroids: general – white dwarfs – methods: analytical

1. Introduction

Over the last 30 yr it has become clear that planetary perturbations can force asteroids into such highly eccentric orbits that they collide with the Sun. There is also growing evidence that planetesimals may fall into their parent stars or suffer tidal disruption.

In the solar system, Sun-grazing long-period comets (e.g. the famous Kreutz group; Marsden 1967) have been known for a long time, but these objects are expected to come from the Oort cloud on orbits that are already highly eccentric, which means that planetary perturbations only play a minor role in driving their final Sun-grazing eccentricities. But in 1994, Farinella et al. (1994), following the evolution of the known near-Earth objects

with numerical simulations, discovered that asteroids frequently collide with the Sun. The original source of near-Earth asteroids is the asteroid belt, so in this case planetary perturbations must play a major role in removing the object's initial angular momentum. Mean motion resonances with Jupiter and a secular resonance with Saturn were identified as the main mechanisms capable of pushing the asteroid's eccentricity to high values, far more effective than planetary close encounters. Gladman et al. (1997), again with numerical simulations, showed that more than 70% of the objects initially in the ν_6 secular resonance with Saturn or the 3:1 mean motion resonance with Jupiter eventually collide with the Sun.

The collision of small bodies with the central star is not an oddity of our solar system. Ferlet et al. (1987) and Lagrange et al. (1987) proposed that the red-shifted Ca II and NA I absorption lines observed in β Pictoris were due to infalling evaporating bodies (see also Beust et al. 1989, 1990, 1991). The

^{*} The Mathematica notebook is only available at the CDS via anonymous ftp to cdsarc.u-strasbg.fr (130.79.128.5) or via <http://cdsarc.u-strasbg.fr/viz-bin/qcat?J/A+A/605/A23>

frequency of such events, on a characteristic timescale of a few years, suggests that the infalling bodies were on short-period orbits, similar to asteroids or short-period comets in the solar system. In recent years, many more young star systems have been observed to possess Doppler-shifted, transient absorption line features similar to β Pic, suggesting that infalling small bodies may be a common phenomenon (e.g. [Sorelli et al. 1996](#); [Welsh & Montgomery 2013](#); [Greaves et al. 2016](#)).

Additional evidence for planetesimals falling into the central star comes from the atmospheric pollution in heavy elements observed in white dwarfs (see [Farihi 2016](#) for a review). Spectroscopic studies of a large sample of cool, hydrogen-rich white dwarfs has established a minimum frequency of 30% for the pollution phenomenon in these objects ([Zuckerman et al. 2003](#); [Koester et al. 2014](#)). In cold white dwarfs, heavy elements should rapidly sink ([Fontaine & Michaud 1979](#); [Vauclair & Fontaine 1979](#)) leaving behind only hydrogen or helium. Thus, external sources must be responsible for any photospheric metals. The most commonly accepted explanation is that these metals originate from tidally disrupted planetesimals ([Debes & Sigurdsson 2002](#); [Jura 2003](#)). In essence, planetesimals perturbed into highly eccentric orbits pass within the stellar Roche limit (which is of the order of the solar radius R_{\odot}) and are torn apart by gravitational tides; subsequent collisions reduce the fragments to dust; the latter produce an infrared excess and slowly rain down onto the stellar surface, which generates the observed atmospheric pollution. Obviously, for this model to work, planetesimals have to be “pushed” by planetary perturbations to achieve orbits that are eccentric enough to pass within $\sim R_{\odot}$ from the star. Given the ubiquity of the white dwarf pollution phenomenon, a robust mechanism of extreme eccentricity excitation of planetesimals is needed (e.g. [Bonsor et al. 2011](#); [Debes et al. 2012](#); [Petrovich & Muñoz 2017](#)). These astrophysical contexts have revived the interest in mean motion resonances with eccentric planets as a generic mechanism for pumping the eccentricities of small bodies from ~ 0 to ~ 1 , i.e. for driving planetesimals into the central star.

Analytic celestial mechanics shows that mean motion resonances with a planet on a *circular* orbit only cause an oscillation of the small body’s semi-major axis coupled with a moderate oscillation of the eccentricity and with the libration of the angle $k\lambda - k'\lambda'$ (where λ and λ' are the mean longitudes of the small body and of the planet, respectively, and the integer coefficients k and k' define the $k':k$ resonance; [Henrard & Lemaître 1983](#); [Lemaître 1984](#)). However, if the perturbing planet has a finite eccentricity, inside a mean motion resonance there can be a dramatic secular evolution; the eccentricity of the small body can undergo large excursions correlated with the precession of the longitude of perihelion ([Wisdom 1985, 1983](#); [Henrard & Caranicolas 1990](#)).

These pioneer works used a series expansion of the Hamiltonian in power laws of the eccentricities of the perturbed body (e) and of the planet (e'), and focused specifically on the case of the 3:1 resonance with Jupiter. A few years later, [Moons & Morbidelli \(1993, 1995\)](#) developed a semi-analytic study of the dynamics in mean motion resonances using a first-order expansion in e' but no series expansions in e . This way, they were able to follow the evolution of the small body to arbitrarily high eccentricities. This approach is valid only for small values of e' and moreover for $e > e'$. Motivated by the [Farinella et al. \(1994\)](#) numerical results, Moons and Morbidelli focused on the specific case of the solar system, including the effects of Saturn on the orbital evolution of Jupiter in addition to their combined perturbation to the asteroid. In this framework,

they established the existence of overlapping secular resonances inside the 4:1, 3:1, 5:2, and 7:3 mean motion resonances, which can push the eccentricity of the small body to unity.

In a more general context, [Beust & Morbidelli \(1996\)](#) investigated the secular dynamics in mean motion resonances with a single planet with various (albeit moderate) eccentricities. Again, they considered an expansion in e' to the first order, and no expansion in the eccentricity of the perturbed body. Of all the resonances, they found that 4:1 is the most powerful in pushing the eccentricity of the small body from ~ 0 to ~ 1 , provided that $e' \gtrsim 0.05$. In contrast, the 3:1 resonance only generates large oscillations in the eccentricity of the small body, but they are insufficient to produce star-grazing orbits, at least for planet eccentricities up to 0.1. Because of the linear expansion in e' , [Beust & Morbidelli \(1996\)](#) could not determine the threshold planetary eccentricity that generates the star-grazing phenomenon for small bodies initially on quasi-circular orbits in the 3:1 resonance.

In this paper we revisit the problem of the eccentricity evolution of small bodies inside mean motion resonances with an eccentric planet using a semi-analytic approach. In order to go beyond the works cited above, we do not expand the Hamiltonian in the eccentricity of either the small body or the perturber. In this way, our study is valid for all eccentricities and also in the $e < e'$ regime. Our work is not the first to avoid expansions in e' (e.g. [Beaugé et al. 2006](#); [Michtchenko et al. 2006](#); [Sidorenko 2006](#)). We use the adiabatic principle (already invoked in [Wisdom 1985](#)) to disentangle the motion related to the libration of $k\lambda - k'\lambda'$ from the secular motion relating eccentricity and longitude of perihelion. To remain relatively simple, our analysis is performed in the limit of small amplitude of libration in the mean motion resonance.

The paper is structured as follows. In Sect. 2, we develop the analytic formalism for the study of the secular dynamics at the core of mean motion resonances, without series expansions. This results in the averaged Hamiltonian with two degrees of freedom (2.10). In Sect. 3 we lay out the method for studying the dynamics given by the averaged Hamiltonian, using the theory of adiabatic invariance; we also discuss the limit of validity of this method. In Sect. 4 we also include a post-Newtonian term, describing the fast precession of the longitude of perihelion at large eccentricity due to General Relativity. Our results are presented in Sect. 5. We first neglect the effect of General Relativity; in this case the secular evolution is independent of the planet’s mass, and only the timescale of the secular evolution depends on it. We focus in particular on the 4:1, 3:1, and 2:1 resonances, and for each of these resonances we evaluate what planetary eccentricities are needed to lift bodies from initially quasi-circular orbits to star-grazing ones, if it is ever possible. When this is the case, we then introduce the post-Newtonian correction, which makes the secular dynamics at high eccentricity dependent on the planetary mass. Thus, we determine – for the resonances and the planetary eccentricities previously considered – the minimal planetary mass required to achieve the star-grazing phenomenon. In addition, we provide supplementary material available at the CDS: a Mathematica notebook implementing our model so that the reader can compute the secular dynamics in the desired resonances with the desired planets. The conclusions of this work are summarized in Sect. 6.

2. Planetary Hamiltonian

We start with the Hamiltonian for the restricted planar three-body problem. By denoting with $\mathbf{x} = (x, y)$ and $\mathbf{v} = (v_x, v_y)$ the

Cartesian coordinates and momenta of the perturbed test particle (“small body”), and using a prime for the perturber (“planet”), the Hamiltonian reads:

$$\begin{aligned} \mathcal{H} &= \mathcal{H}_{\text{kepl}} + \mathcal{H}_{\text{pert}} \\ &= \frac{\|\mathbf{v}\|^2}{2} - \frac{\mathcal{G}M_*}{\|\mathbf{x}\|} - \mathcal{G}m' \left(\frac{1}{\Delta} - \frac{\mathbf{x} \cdot \mathbf{x}'}{\|\mathbf{x}'\|^3} \right), \end{aligned} \quad (2.1)$$

where M_* is the mass of the star, m' is the mass of the perturber, and $\Delta = \|\mathbf{x} - \mathbf{x}'\|$ is the distance between the test particle and the perturber (Murray & Dermott 2000). The perturber is assumed to follow a given Keplerian orbit, so \mathbf{x}' is a function of time. In terms of orbital elements, the Cartesian coordinates are given by

$$\begin{aligned} x &= a(\cos E - e) \cos \varpi - a\sqrt{1-e^2} \sin E \sin \varpi, \\ y &= a(\cos E - e) \sin \varpi + a\sqrt{1-e^2} \sin E \cos \varpi, \end{aligned} \quad (2.2)$$

where a is the semi-major axis, e is the eccentricity and E is the eccentric anomaly of the perturbed particle, and similar (primed) equations and orbital parameters for the perturber (Murray & Dermott 2000).

We introduce the canonical modified Delaunay action-angle variables (Λ, P, λ, p) , given by

$$\begin{aligned} \Lambda &= \sqrt{\mathcal{G}M_*a}, & \lambda &= \ell + \varpi, \\ P &= \sqrt{\mathcal{G}M_*a}(1 - \sqrt{1-e^2}), & p &= -\varpi, \end{aligned} \quad (2.3)$$

where λ is the mean longitude, $\ell = E - e \sin E$ is the mean anomaly, and ϖ is the longitude of pericentre of the test mass. In order to make the system autonomous, we extend the phase space by introducing for the perturber

$$\Lambda', \quad \lambda' = \ell' + \varpi' = n'(t - t_0), \quad (2.4)$$

where $n' = \sqrt{\mathcal{G}(M_* + m')/a'^3}$ is the mean motion of the perturber. We assume that the perturber does not precess, so without loss of generality we set $\varpi' = 0$. Now the autonomous Hamiltonian of the system reads

$$\begin{aligned} \mathcal{H}(\Lambda, P, \Lambda', \lambda, p, \lambda') &= -\frac{\mathcal{G}^2 M_*^2}{2\Lambda^2} + n' \Lambda' \\ &+ \mathcal{H}_{\text{pert}}(\Lambda, P, \lambda, p, \lambda'; e', \varpi' = 0), \end{aligned} \quad (2.5)$$

where the perturbation part $\mathcal{H}_{\text{pert}}$ is to be written in terms of the newly defined variables. We note that it depends parametrically on the arbitrary values of e' and $\varpi' = 0$.

We now consider the test particle to be close to an inner mean motion resonance with the outer perturber. In other words, we assume $kn - k'n' \sim 0$, where $n = \sqrt{\mathcal{G}M_*/a^3}$ is the mean motion of the test particle for some positive integers k, k' , such that $k' > k$. In order to study the resonant dynamics, it is possible to introduce a set of canonical resonant action-angle variables:

$$\begin{aligned} S &= P, & \sigma &= \frac{k'\lambda' - k\lambda + (k' - k)p}{(k' - k)}, \\ N &= \frac{k' - k}{k}\Lambda + P, & \nu &= \frac{-k'\lambda' + k\lambda}{(k' - k)} = -\sigma + p, \\ \tilde{\Lambda}' &= \Lambda' + \frac{k'}{k}\Lambda, & \tilde{\lambda}' &= \lambda'. \end{aligned} \quad (2.6)$$

The historical reason for adopting these variables is that for $e' = 0$ there is no harmonic term in ν in the Hamiltonian and

thus N is a constant of motion. The reason why the critical resonant angle σ is not simply defined as $k'\lambda' - k\lambda + (k' - k)p$ is explained in Lemaître (1984) and is due to the d'Alembert rules: the coefficient of the terms $\cos[(k'\lambda' - k\lambda + (k' - k)p)]$ in the Fourier expansion of the perturbing Hamiltonian is proportional to $e^{|k' - k|}$ for small values of e . Thus, for small eccentricities the Hamiltonian is a polynomial expression in $e \cos \sigma$ and $e \sin \sigma$, and the apparent singularity at $e = 0$ can be removed.

Using the variables (2.6), the Keplerian part of the Hamiltonian takes the form

$$\begin{aligned} \mathcal{H}_{\text{kepl}}(S, N, \tilde{\Lambda}') &= -\mathcal{G}^2 M_*^2 \frac{(k' - k)^2}{2k^2(N - S)^2} \\ &+ n' \left[\tilde{\Lambda}' - \frac{k'}{(k' - k)}(N - S) \right]. \end{aligned} \quad (2.7)$$

At this point, we average the Hamiltonian over the fast angles. From a computational point of view, a remark is in order. The Cartesian components given in (2.2) are expressed in terms of the eccentric anomalies E, E' . Thus, it would be necessary to invert Kepler's equation $\lambda - \varpi = \ell = E - e \sin E$ to obtain $E = E(\lambda)$, and similarly for $E' = E'(\lambda')$. If e' is not too large, the latter inversion is not problematic. However the eccentricity e of the test particle can reach high values, and solving the Kepler equation for the test particle becomes numerically cumbersome. Therefore, it is advisable to retain the dependence on the eccentric anomaly E , use the differential relationship $d\lambda = (1 - e \cos E) dE$, and integrate over E instead. This is more convenient because the dependence of λ on E is given through Kepler's equation by an explicit formula. We also note that λ is related to λ' through σ by $\lambda' = [(k\lambda - (k' - k)(p - \sigma))]/k'$. In summary, using the resonant relationship and Kepler's equation one obtains E' from λ' , λ' from λ , and λ from E , so that the averaging on E eliminates the short periodic dependence of the Hamiltonian. By doing so, the canonical angle λ' vanishes from the averaged Hamiltonian, and $\tilde{\Lambda}'$ becomes a constant of motion, so that the term $n' \tilde{\Lambda}'$ can be dropped from (2.7).

Proceeding this way, we have that

$$\bar{\mathcal{H}}_{\text{pert}}(S, N, \sigma, \nu) := \frac{1}{2\pi k'} \int_0^{2\pi k'} \mathcal{H}_{\text{pert}}(1 - e \cos E) dE; \quad (2.8)$$

it is important to note that we integrate over E from 0 to $2\pi k'$ instead of just 2π because only after k' revolutions of the test particle around the star (which correspond to k revolutions of the outer perturber) does the system attain the initial configuration, thus recovering the complete periodicity of the Hamiltonian. The integral (2.8) can be solved numerically. In our code we use a Mathematica function with an imposed relative accuracy of 10^{-10} . For the Keplerian part we just write

$$\bar{\mathcal{H}}_{\text{kepl}}(S, N) := -\mathcal{G}^2 M_*^2 \frac{(k' - k)^2}{2k^2(N - S)^2} - n' \frac{k'}{(k' - k)}(N - S). \quad (2.9)$$

The averaged Hamiltonian then becomes

$$\bar{\mathcal{H}}(S, N, \sigma, \nu) := \bar{\mathcal{H}}_{\text{kepl}} + \bar{\mathcal{H}}_{\text{pert}}. \quad (2.10)$$

This two degree of freedom system is not integrable in general, unless further approximation is made.

3. Studying the averaged Hamiltonian

We now intend to study quantitatively the dynamics given by the Hamiltonian (2.10). This can be seen as an integrable system

(i.e. the Keplerian part), to which a small perturbation of order $\mu = m'/M_* \ll 1$ is added.

We begin by noticing that $\bar{\mathcal{H}}_{\text{kepl}}$ only depends on $N - S$, so it is convenient to introduce the canonical variables

$$\begin{aligned} \Sigma &= S - N, & \sigma, \\ N, & & p = \sigma + \nu, \end{aligned} \quad (3.1)$$

making $\bar{\mathcal{H}}_{\text{kepl}}$ a function of Σ alone. The location of exact resonance is given by the value $\Sigma = \Sigma_{\text{res}}$ such that

$$\frac{\partial \bar{\mathcal{H}}_{\text{kepl}}}{\partial \Sigma}(\Sigma_{\text{res}}) = 0, \quad \text{i.e. } \Sigma_{\text{res}} = -(\mathcal{G}M_*)^{2/3} \frac{(k' - k)}{(k^2 k' n')^{1/3}}, \quad (3.2)$$

which is simply $n = n_{\text{res}} = (k'/k)n'$. The expansion of $\bar{\mathcal{H}}_{\text{kepl}}$ in $\Delta\Sigma = \Sigma - \Sigma_{\text{res}}$ starts with a quadratic term in $\Delta\Sigma$. Since the perturbation $\bar{\mathcal{H}}_{\text{pert}}$ is a function of (Σ, N, σ, p) and is of order μ , the dynamics in the canonical pair of variables (Σ, σ) near Σ_{res} is equivalent to that of a pendulum with Hamiltonian of the form $(\Delta\Sigma)^2 + \mu \cos \sigma$, so its frequency is of order $\sqrt{\mu}$. On the other hand, the dynamics in the canonical pair (N, p) is slower, with a characteristic frequency of order μ . We can therefore apply the adiabatic principle and study the dynamics in (Σ, σ) with fixed (N, p) , and then the dynamics in (N, p) keeping constant the action integral

$$J = \oint \Sigma d\sigma, \quad (3.3)$$

which is the adiabatic invariant of the dynamics (Henrard 1993).

We now explain this procedure in more detail. Once the values of N and p have been fixed, $\bar{\mathcal{H}}$ reduces to a one degree of freedom Hamiltonian in (Σ, σ) and parametrized by (N, p) , which we denote by $\bar{\mathcal{H}}_{(N,p)}(\Sigma, \sigma)$. This Hamiltonian is therefore integrable, so we can study its dynamics by plotting its level curves. We note however that by fixing N we can obtain Σ from e and vice versa, so we can also use $(e \cos \sigma, e \sin \sigma)$ as independent variables. Although these variables are not canonical, they have the already mentioned advantage that for small e the Hamiltonian is a polynomial in $(e \cos \sigma, e \sin \sigma)$, so the level curves do not have a singularity at $e = 0$. In addition, the plot of the level curves does not require the use of canonical variables. We show examples of these plots in the case of the 4:1 resonance in Fig. 1.

In principle, the dynamics can be studied for any value of J . Once the cycle of $\bar{\mathcal{H}}_{(N,p)}(\Sigma, \sigma)$ corresponding to the considered value of J through (3.3) is identified, the full Hamiltonian $\bar{\mathcal{H}}(\Sigma, \sigma, N, p)$ is averaged over the cycle, as explained in Henrard (1993), leading to a new one degree of freedom Hamiltonian $\bar{\bar{\mathcal{H}}}(N, p; J)$. This Hamiltonian is integrable, and the resulting dynamics in (N, p) describes the secular evolution of the small body inside the mean motion resonance with the perturber.

In this paper we vastly simplify this procedure by limiting ourselves to the case $J \rightarrow 0$, i.e. the limit of small libration amplitude in the mean motion resonance. In this limit, the cycle in (Σ, σ) described by $\bar{\mathcal{H}}_{(N,p)}$ shrinks to the stable equilibrium point. Thus, there is no need to average the full Hamiltonian over a cycle: $\bar{\bar{\mathcal{H}}}(N, p; J = 0)$ is obtained by evaluating $\bar{\mathcal{H}}$ on the stable equilibrium point of $\bar{\mathcal{H}}_{(N,p)}$ in the variables e and σ . We note that by having fixed N , we are effectively linking the semi-major axis a to the eccentricity e , via the relation

$$a = \frac{N^2}{\mathcal{G}M_* (k'/k - \sqrt{1 - e^2})^2}; \quad (3.4)$$

therefore, we recover the equilibrium values a_{eq} of the semi-major axis as well.

We show an example of this calculation in Fig. 2, for the 2:1, 3:1, and 4:1 resonances. It is worth pointing out that the equilibrium points in the (e, a) diagram deviate away from the Keplerian resonant value $a_{\text{res}} = a'(k/k')^{2/3}$ as $e \rightarrow 0$. This is especially evident in the case of first-order resonances, $|k - k'| = 1$. In this case, for $e > e'$ the main harmonic in the Hamiltonian is $e \cos \sigma$, i.e. $\sqrt{P} \cos \sigma$, from (2.3) and expansion for small e . Because $\dot{p} = \partial \mathcal{H} / \partial P$, this harmonic gives $\dot{p} \propto 1/\sqrt{P} \sim 1/e$, which grows considerably as e approaches zero; therefore, in order to maintain $\dot{\sigma} = [k'\lambda' - k\lambda + (k' - k)\dot{p}]/(k' - k) \sim 0$, it is necessary to have $k'\lambda' - k\lambda \neq 0$ i.e. $a/a' \neq (k/k')^{(2/3)}$. For resonances of order $|k' - k| > 1$ the main harmonic in the Hamiltonian for $e > e'$ is $e^{|k' - k|} \cos \sigma$, i.e. $P^{|k' - k|/2} \cos \sigma$. Therefore, the first derivative in P is not singular for $e \sim \sqrt{P} \rightarrow 0$. However, for $e < e'$ the main harmonic dependent on e is $e'^{|k' - k| - 1} e \cos[(k' - k)\sigma - (k' - k - 1)(p + \varpi)]$, which gives a contribution to \dot{p} proportional to $1/e$, and the same reasoning applies. Indeed, in the case of inner mean motion resonance, a_{eq} always attains values that are slightly less than the Keplerian a_{res} as $e \rightarrow 0$, as shown in Fig. 2. We must note, however, that the deviation of the equilibrium points away from the resonant value a_{res} indicates a rapid precession of the pericentre ϖ . This means that our assumption that p and N remain constant is no longer valid. It breaks down when their motion evolves with a frequency of order $\sqrt{\mu}$, i.e. of the same order as the frequency of the Σ, σ evolution. When $\dot{p} \sim \sqrt{\mu}$, the equilibrium semi-major axis of the test particle deviates from the Keplerian value by the amount of order $(2/3)(\sqrt{\mu}/k)(a_{\text{res}})^{5/2}$. Thus, we can determine the lower limit in eccentricity for the validity of our approach as the value of e at which the equilibrium point a_{eq} deviates away from a_{res} by more than this quantity. In this paper, we will focus mainly on resonances of order higher than 1 because they are much more efficient in pushing the eccentricity e from ~ 0 to ~ 1 (see Sect. 5). In this case, for $e < e'$ our approach is valid down to very small values of the eccentricity.

We have implemented this scheme in a Mathematica notebook, which is made available at the CDS. Let us now briefly explain the steps in our calculation, which ultimately yields the level curves of the Hamiltonian $\bar{\bar{\mathcal{H}}}(N, p; J = 0)$ on the $(e \cos \varpi, e \sin \varpi)$ plane, thereby describing the secular evolution of the small body inside the mean motion resonance with the perturber, in the limit of $J = 0$. First, we consider a fixed value of $N = N^*$. For some given value of ϖ , we can find the (stable) equilibrium point in the $(e \cos \sigma, e \sin \sigma)$ plane in the following manner. If $\varpi = \varpi_0 = 0$, the Hamiltonian (2.10) contains only cosines of $(k' - k)\sigma$ (and its multiples) so that its extrema in σ are found at $2\pi l/(k' - k)$ and $(2\pi l + \pi)/(k' - k)$, $l \in \mathbb{Z}$. Taking for example $\sigma = \sigma_0 = 0, \pm\pi$, we can write the Hamiltonian (2.10) as $\bar{\mathcal{H}}(e, N^*, \sigma_0, \varpi_0)$ and we can find its maximum as a function of the eccentricity. The fact that $\bar{\mathcal{H}}$, as a function of e , must have a maximum at the resonance can be seen from Eq. (2.9), which clearly has a maximum in $\Sigma = S - N$ at Σ_{res} (defined in Eq. (3.2)). Then, because $\frac{\partial^2 \mathcal{H}}{\partial \Sigma^2} = \frac{\partial^2 \mathcal{H}}{\partial S^2}$ and S is monotonic in e , $\bar{\mathcal{H}}$ must have a maximum in e . We call e_{max} the value of the eccentricity for which $\bar{\mathcal{H}}$ is maximal. We must now check that this is in fact the stable equilibrium point, i.e. that in σ_0 the function $\bar{\mathcal{H}}(e_{\text{max}}, N^*, \sigma, \varpi_0)$ of σ has a maximum (and not a minimum). If this is not the case, we can repeat the calculation with $\sigma = \pi/(k' - k), \pi/(k' - k) + \pi$. Although in principle the maximum in σ could be away from this axis (because of the higher order harmonics in $(k' - k)\sigma$), in practice in all the cases we studied

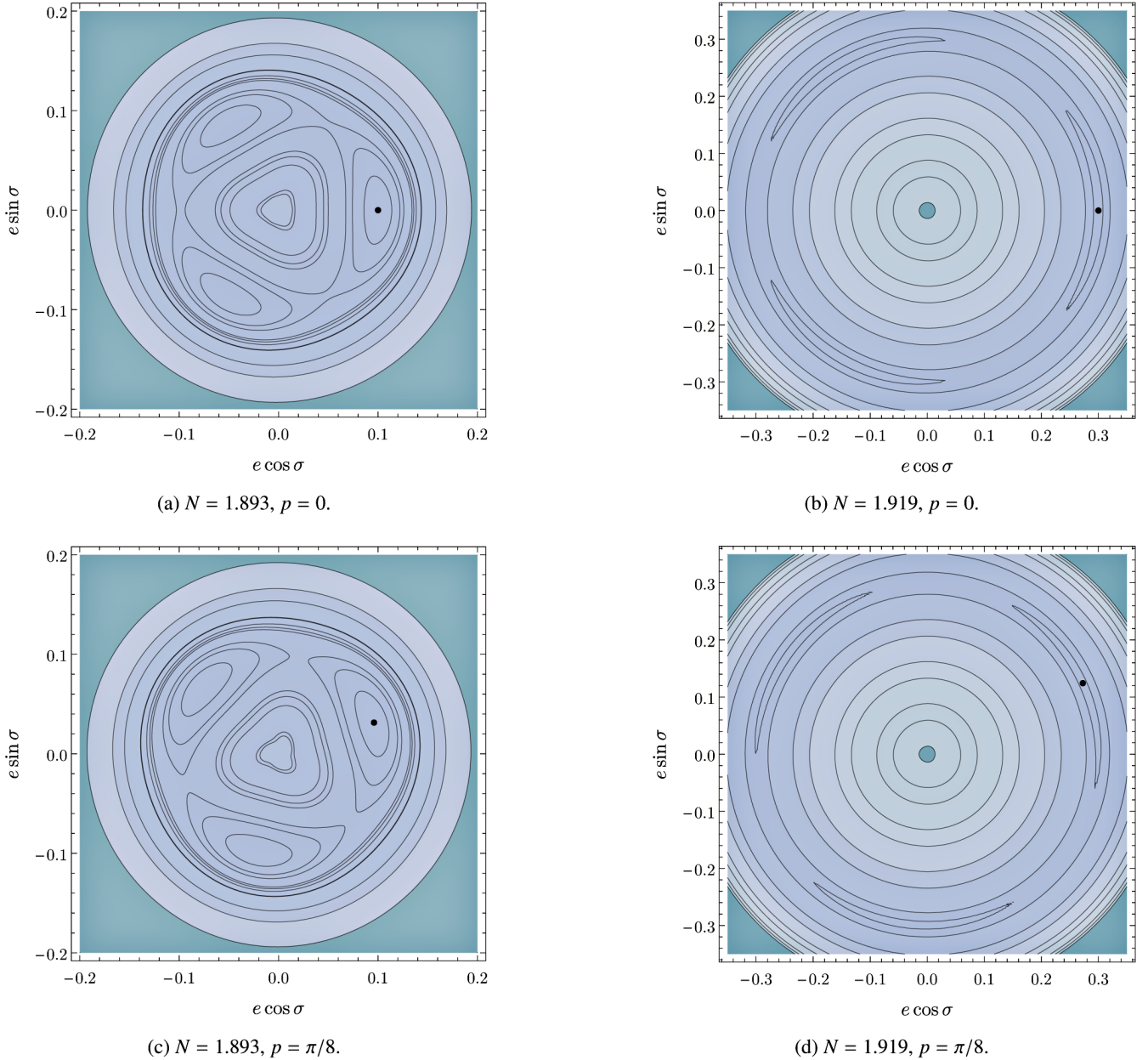


Fig. 1. Level plots of the Hamiltonian $\bar{\mathcal{H}}_{(N,p)}(\Sigma, \sigma)$ on the $(e \cos \sigma, e \sin \sigma)$ plane for different N and p . This is the case of $k' = 4, k = 1$, with $e' = 0.1, a' = 1$ AU, and $\mu = 10^{-3}$ for the perturber (in units where $\mathcal{G}M_s = 1$). The black dot in each panel indicates the position of the stable equilibrium point that is found by our algorithm. The function $\bar{\mathcal{H}}_{(N,p)}$ is periodic in σ with period $2\pi/(k' - k)$, so there will always be $k' - k$ equivalent stable equilibria one rotation away from each other. We note that e_{eq} increases with N , while p has the effect of simply rotating the diagram.

this procedure effectively yields, for the given value of $N = N^*$ and for $\varpi = \varpi_0 = 0$, the stable equilibrium point in (e, σ) , denoted by $(e_{\text{eq}}, \sigma_{\text{eq}})$. We note from Fig. 1 that e_{eq} increases with the value N^* .

Following the procedure described above, we can assign to the Hamiltonian $\bar{\mathcal{H}}(N^*, \varpi_0; J = 0)$ the value $\bar{\mathcal{H}}(e_{\text{eq}}, N^*, \sigma_{\text{eq}}, \varpi_0)$ on the point $(e_{\text{eq}} \cos \varpi_0, e_{\text{eq}} \sin \varpi_0)$. We also note that from the equilibrium value e_{eq} , it is possible to obtain the corresponding a_{eq} through Eq. (3.4). When ϖ is not zero, the diagram in the $(e \cos \sigma, e \sin \sigma)$ plane is, to a good approximation¹ for most values of e , simply rotated by a quantity related to ϖ , so that the

¹ We have checked that in the 4:1 resonance e_{eq} changes only by $\lesssim 0.1\%$ with the rotation of ϖ , down to $e_{\text{eq}} \sim 0.05$, for $e' = 0.1$.

equilibrium values of the eccentricity and the semi-major axis do not change substantially, but only σ_{eq} changes (see Fig. 1). This way, it is possible to obtain the equilibrium value for σ by finding the maximum in σ of the function $\bar{\mathcal{H}}(e_{\text{eq}}, N^*, \sigma, \varpi)$ for the fixed value of ϖ . It is worth noticing that in order to assign to the point $(e_{\text{eq}} \cos \varpi, e_{\text{eq}} \sin \varpi)$ the appropriate value of the Hamiltonian, we are only interested in the $\max_{\sigma \in [0, 2\pi]} \bar{\mathcal{H}}(e_{\text{eq}}, N^*, \sigma, \varpi) = \max_{\sigma \in [0, 2\pi/(k' - k)]} \bar{\mathcal{H}}(e_{\text{eq}}, N^*, \sigma, \varpi)$ for the fixed value of ϖ , not in the actual value σ_{eq} of σ where the maximum is attained. However, we need to check that σ_{eq} changes smoothly with N^* and ϖ . If this were not the case, a bifurcation would occur, which would invalidate the assumption that the amplitude of libration remains small. We have checked that this happens only in the case of the

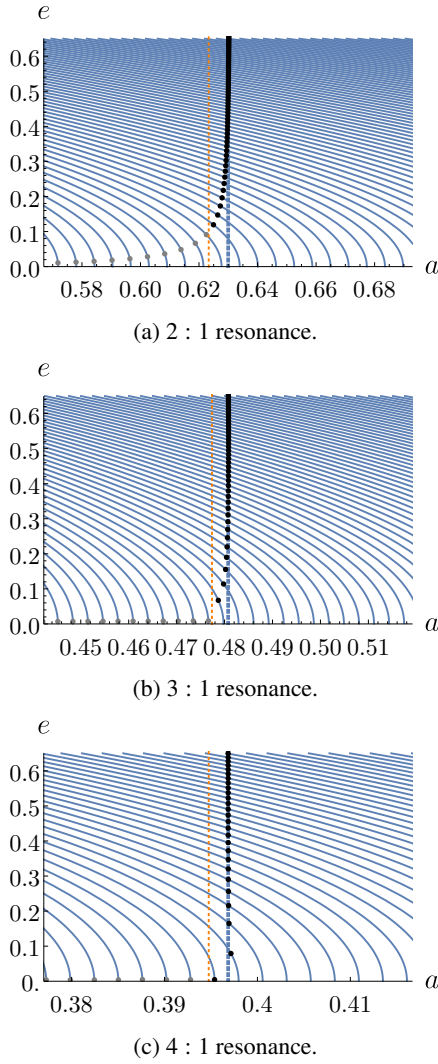


Fig. 2. Level curves of N on the (a, e) plane for the case of the 2:1, 3:1, and 4:1 resonances with $a' = 1$ AU for the perturber (in units where $\mathcal{G}M_* = 1$). The solid lines depict Eq. (3.4), where the numerical value of N increases from left to right. The vertical thick dashed lines indicate the location of exact Keplerian resonance, $a_{\text{res}} = a'(k/k')^{2/3}$. The dots represent the equilibrium values for the eccentricity and the semi-major axis on different level curves of N , while the arbitrary value of ϖ remains fixed. Here we used $e' = 0.2$ and $\mu = 10^{-3}$. We note that the equilibrium points deviate away from exact resonance at low eccentricities, which is particularly evident in the case of first-order resonances (the 2:1 resonance in this case; see text for details). Since this deviation is linked to a faster precession of the pericentre $\dot{\varpi} = -p$, the value of e at which this effect becomes higher than $(2/3)(\sqrt{\mu}/k)(a_{\text{res}})^{5/2}$ yields a lower bound in e above which our approach is valid. The orange dashed line indicates a deviation from the exact resonance of this amount. We thus colour-coded the equilibrium points using black for those that fall above this lower limit in eccentricity, and grey for those that fall below it: for the latter, the fast change in p does not allow us to consider the pair (N, p) as slowly evolving variables.

3:1 resonance in a point on the $\varpi = 0$ axis (e.g. at $e \simeq 0.35$ in Fig. 7b). We note that this point is never crossed during the secular evolution because it appears as a centre of libration.

By letting N vary, i.e. effectively by allowing e_{eq} to vary, we obtain the level curves of the Hamiltonian $\bar{\mathcal{H}}(N, p; J = 0)$ in the variables $(e \cos \varpi, e \sin \varpi)$. We present several examples

in Sect. 5, where we show level curves of $\bar{\mathcal{H}}$ for different resonances and different values of e' .

4. Effect of short-range forces

When the eccentricity of the test mass reaches values close to 1, so that the osculating ellipse becomes narrower and narrower, the periastron distance from the star $a_{\text{peri}} = a(1 - e)$ becomes considerably small. At this point, the effect of various short-range forces may become important and must be considered. One such short-range force arises from General Relativity, with the post-Newtonian contribution to the test particle's Hamiltonian given by

$$\mathcal{H}_{\text{GR}} = \frac{\mathcal{G}M_*}{a} \left(\frac{\mathcal{G}M_*}{ac^2} \right) \left(\frac{15}{8} - \frac{3}{\sqrt{1-e^2}} \right), \quad (4.1)$$

where c is the speed of light (Krivov 1986). We note that the $15/8$ term only gives the General Relativity correction to the mean motions, while the $1/\sqrt{1-e^2}$ term gives the correction to the precession of the pericentre. Since we are only interested in the latter and we have averaged over the mean motion, we drop the former. Another short-range force arises from the rotational bulge of the central star, with the Hamiltonian given by

$$\mathcal{H}_{\text{rot}} = -\frac{\mathcal{G}M_*R_*^2J_2}{2a^3(1-e^2)^{3/2}}, \quad (4.2)$$

where R_* is the stellar radius, and $M_*R_*^2J_2$ is the rotation-induced quadrupole moment of the star. To assess the importance of these short-range forces, we compare \mathcal{H}_{GR} and \mathcal{H}_{rot} to Φ_0 , the characteristic tidal potential produced by the planetary perturber on the test particle,

$$\Phi_0 \equiv \frac{\mathcal{G}m'a^2}{a'^3}. \quad (4.3)$$

We find

$$\begin{aligned} \frac{|\mathcal{H}_{\text{GR}}|}{\Phi_0} &\simeq 10^{-2} \left(\frac{M_*}{M_\odot} \right)^2 \left(\frac{m'}{M_\oplus} \right)^{-1} \left(\frac{a'}{a} \right)^3 \\ &\times \left(\frac{a}{\text{AU}} \right)^{-1} \frac{1}{(1-e^2)^{1/2}} \\ &\simeq 1.7 \left(\frac{M_*}{M_\odot} \right)^2 \left(\frac{m'}{M_\oplus} \right)^{-1} \left(\frac{n}{4n'} \right)^2 \\ &\times \left(\frac{a}{\text{AU}} \right)^{-1/2} \left(\frac{a_{\text{peri}}}{R_\odot} \right)^{-1/2}, \end{aligned} \quad (4.4)$$

$$\begin{aligned} \frac{|\mathcal{H}_{\text{rot}}|}{\Phi_0} &\simeq \frac{k_{q*}\hat{\Omega}_*^2}{2} \left(\frac{M_*}{m'} \right) \left(\frac{R_*}{a} \right)^2 \left(\frac{a'}{a} \right)^3 \frac{1}{(1-e^2)^{3/2}} \\ &\simeq 0.086 \left(\frac{k_{q*}}{0.01} \right) \left(\frac{P_*}{10 \text{ day}} \right)^{-2} \left(\frac{R_*}{R_\odot} \right)^5 \left(\frac{m'}{M_\oplus} \right)^{-1} \\ &\times \left(\frac{n}{4n'} \right)^2 \left(\frac{a}{\text{AU}} \right)^{-1/2} \left(\frac{a_{\text{peri}}}{R_\odot} \right)^{-3/2}, \end{aligned} \quad (4.5)$$

where $a_{\text{peri}} = a(1-e)$, and we use $J_2 = k_{q*}\hat{\Omega}_*^2 = k_{q*}\Omega_*^2R_*^3/(GM_*)$, with $\Omega_* = 2\pi/P_*$ the stellar rotation rate. Clearly, for most main-sequence stars (with $P_* \gtrsim 2$ days) and white dwarfs, $|\mathcal{H}_{\text{rot}}|$ is negligible compared to $|\mathcal{H}_{\text{GR}}|$. We neglect \mathcal{H}_{rot} in the remainder of this paper.

It is straightforward to include \mathcal{H}_{GR} into the scheme outlined in Sect. 3 as we simply need to add the value $\mathcal{H}_{\text{GR}}(a_{\text{eq}}, e_{\text{eq}})$ to the value of the planetary Hamiltonian. This could change the dynamics of the system considerably at sufficiently high eccentricity. In fact, up to this point, the perturber's mass (rescaled by the star's mass) μ has played a role in setting the amplitude of libration in Σ (or a, e) in the Hamiltonian $\bar{\mathcal{H}}_{(N,p)}$, and in setting the frequency of libration around the stable equilibrium point. However, the dynamics described by $\bar{\mathcal{H}}(N, p; J = 0)$ does not depend on the perturber's mass because both N and p appear only in the part of the Hamiltonian derived from $\bar{\mathcal{H}}_{\text{pert}}$, where μ is a multiplying parameter. Thus, the evolution of e as a function of $\varpi = -p$ does not depend on μ , only the timescale of this evolution does (and scales as $1/\mu$).

With the addition of the General Relativity term in the Hamiltonian, the dynamical behaviour of the system will in general depend on μ . Indeed, \mathcal{H}_{GR} is independent of μ , and is dependent on N :

$$\mathcal{H}_{\text{GR}}(\Sigma, N, \sigma, p) = \frac{3\mathcal{G}^4 M_*^4}{c^2} \frac{(k' - k)^4}{k^3 \Sigma^3 (kN - (N + \Sigma)k')}. \quad (4.6)$$

Thus, the actual evolution of N (i.e. of e_{eq} if $J = 0$) as a function of p (i.e. ϖ) depends on the value of μ .

Another way to understand this is that the General Relativity potential has the effect of keeping the eccentricity constant while the pericentre $\varpi = -p$ precesses (because $\dot{p} = \frac{\partial \mathcal{H}_{\text{GR}}}{\partial N} = -\frac{3\mathcal{G}^4 M_*^4}{c^2} \frac{(k' - k)^5}{k^3 \Sigma^3 (kN - (N + \Sigma)k')^2} < 0$ while $\dot{N} = 0, \dot{\Sigma} = 0$). In contrast, in the restricted three-body problem (see previous section) the precession of the pericentre is coupled with the variation in the eccentricity. Since the mass of the perturber μ appears in the planetary potential as a multiplicative factor in the perturbation, but not in the General Relativity potential, it will play the role of a parameter regulating which of the two dynamics in the $(e \cos \varpi, e \sin \varpi)$ plane is dominant. The smaller μ is, the more the General Relativity contribution will prevail, and the less efficient the planet will be in pumping the eccentricity of the test particle; the bigger μ is, the less the \mathcal{H}_{GR} contribution will be apparent.

5. Results

In Figs. 3–5 we show the level curves of the Hamiltonian $\bar{\mathcal{H}}$ (see Sect. 3) on the $(e \cos \varpi, e \sin \varpi)$ plane for the 2:1, 3:1, and 4:1 resonances, respectively, with low values of the eccentricity of the perturber, $e' = 0.05$ and $e' = 0.1$. The General Relativity effect is not included in these figures. The white shaded disks centred at the origin (barely visible in Fig. 5) indicate the regions where the adiabatic method is not valid (see Sect. 3); in these regions our calculations do not necessarily reflect the true dynamics of the system.

We note in Fig. 5 how even for low values of e' the 4:1 resonance is extremely effective in driving the eccentricity of the test particle from $e \sim 0$ to $e \sim 1$. Indeed, there is only a small portion of the phase space that allows orbits starting with low eccentricities to circulate near the origin ($e = 0$). In the case of $e' = 0.05$ only some orbits with moderate initial eccentricities, i.e. $e > 0.2$ and initial $\varpi \sim 0$, actually librate around the stable equilibrium point at $\varpi = 0, e \sim 0.4$, while for $e' = 0.1$, all orbits sufficiently distant from the origin eventually end up at $e \sim 1$. This is not the case for the other resonances. For the 2:1 resonance, we see from Fig. 3 that all orbits with initial eccentricities up to ~ 0.4 and ~ 0.3 , for $e' = 0.05$ and $e' = 0.1$, respectively,

remain confined around the equilibrium point near the origin. Another equilibrium point is present at $e \sim 0.7, \varpi = 0$, implying that whatever the initial values of ϖ even a higher initial eccentricity is not enough to push the test particle to a star-grazing orbit. Indeed, the presence of the separatrix (shown as a black dashed curve) does not allow any orbit with initial eccentricity lower than ~ 0.9 to move farther away from the origin. In the case of the 3:1 resonance, Fig. 4 shows that eccentricities lower than 0.4 for $e' = 0.05$ and 0.2 for $e' = 0.1$ remain small, because the level curves librate around $\varpi = 0$. For $e' = 0.05$ a separatrix bounds the maximum attainable eccentricity as in the 2:1 resonance. This confirms the results in [Beust & Morbidelli \(1996\)](#).

Figures 6–8 depict our results for high values of the perturber's eccentricity, $e' = 0.2$ and $e' = 0.3$. We find that for the 2:1 and 3:1 resonances, even these higher values of e' are not sufficient to generate star-grazing objects from $e \sim 0$. Although for some initial configurations it is possible to observe an excitation in the eccentricity (see e.g. the case of the 3:1 resonance in Fig. 7a, where particles with $e \sim 0.2$ and $\varpi = \pi$ may indeed reach $e \sim 1$), a modest/high initial eccentricity of the test particle is needed in order to eventually reach a value close to 1. On the other hand, Fig. 8 shows that when the perturber's eccentricity is too high, the capability of the 4:1 resonance to raise the eccentricity of the test particle from ~ 0 to ~ 1 is diminished. In all cases (Figs. 6–8), a separatrix confines all orbits close to the origin. We note that this separatrix occupies the region where the adiabatic method remains valid (see Sect. 3), i.e. outside the white shaded region in each plot. Therefore, any orbit with a small initial eccentricity remains confined to low values of e .

As we noted in Sect. 4, when the eccentricity of the test particle reaches sufficiently high values, the effect of the General Relativity term becomes important, and the mass parameter μ plays a crucial role in shaping the dynamics of the system. Led by our results shown in Figs. 3–8, we restrict ourselves to the case of a test particle in the 4:1 mean motion resonance with the outer perturber, and we study the critical value μ_{crit} needed such that the periastron distance $a_{\text{peri}} = a(1 - e)$ reaches sufficiently small values, e.g. the radius of the central star or the star's Roche limit (which is $\sim R_{\odot}$, for white dwarfs and asteroids with internal density about a few g/cm^3).

In Fig. 9 we show the level curves of the Hamiltonian $\bar{\mathcal{H}}$ with $e' = 0.1$, on the $(\varpi, \log a_{\text{peri}})$ plane, both with and without the addition of the General Relativity contribution, for the case of $\mu = 3 \times 10^{-6}$. Here we choose the resonance location of the test particle a_{res} at 1 AU. We can clearly see that while in the purely planetary case the resonance is capable of pushing a test mass with a small initial eccentricity $e \sim 0.05$ into a star-grazing orbit, this does not hold true when \mathcal{H}_{GR} is introduced. In Fig. 10 we repeat the calculation, this time with $\mu = 5 \times 10^{-5}$ and the same values for $a_{\text{res}} = 1$ AU and $e' = 0.1$, and we see that even with the General Relativity contribution, test particles with initial small eccentricities are just about able to reach $a_{\text{peri}} \sim R_{\odot}$. Because the thick curve in Fig. 10b is almost tangent to the bottom of the figure at $\varpi = \pi$, we deduce that the critical mass to achieve star-grazing orbits for this choice of a' and e' is close to 5×10^{-5} solar masses.

The critical perturber mass $\mu_{\text{crit}} = m'_{\text{crit}}/M_*$ can be estimated as follows. For a test particle near a given mean-motion resonance (4:1) with an external perturber (of given m', a', e'), the ‘‘secular’’ planetary Hamiltonian can be written schematically as

$$\bar{\mathcal{H}} = -\Phi_0 \hat{\mathcal{H}}(e, \varpi), \quad (5.1)$$

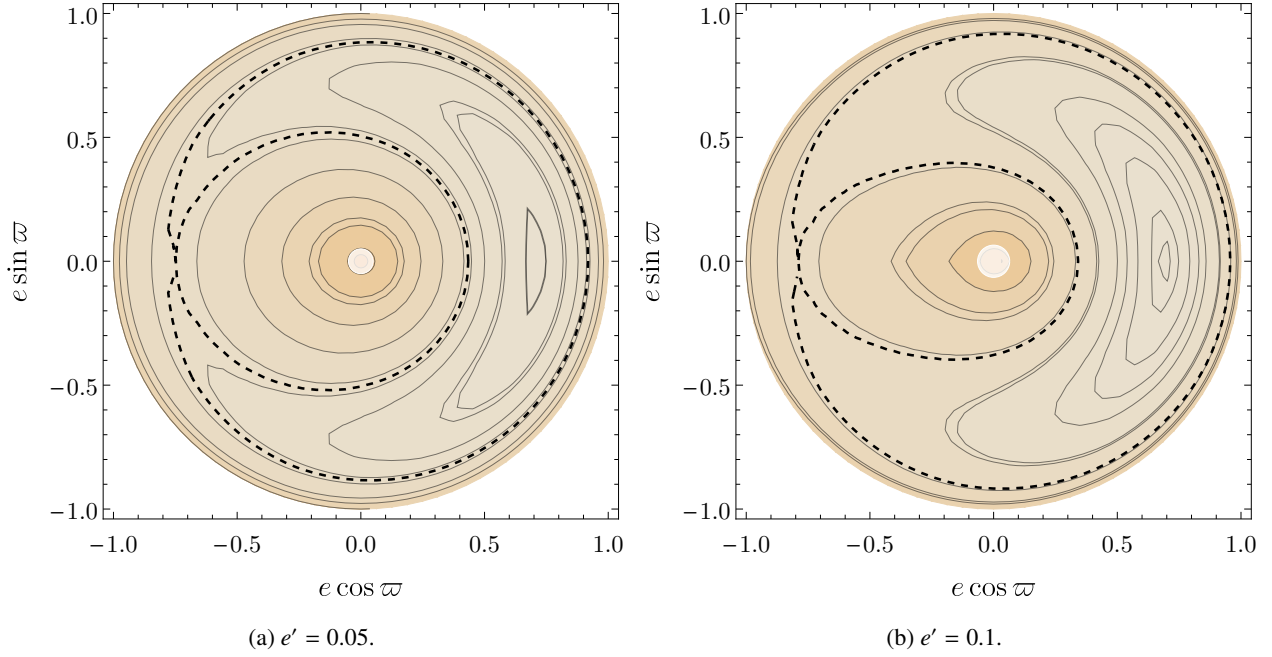


Fig. 3. Level curves of the Hamiltonian $\bar{\mathcal{H}}$ on the $(e \cos \varpi, e \sin \varpi)$ plane for the 2:1 mean motion resonance with an outer perturber for low values of e' ($=0.05$ and 0.1 , both with $\varpi' = 0$). The General Relativity effect is not included. Lighter colours indicate a higher value of the Hamiltonian. The white shaded disks centred at the origin indicate the regions where the adiabatic method is not valid (see Sect. 3), i.e. where our calculations do not necessarily reflect the true dynamics of the system. The dark dashed line indicates a set of critical orbits which separate the phase space into a circulation zone near the origin, a libration zone near the stable equilibrium point at $\varpi = 0$, and an outer circulation region. All orbits with initially low eccentricities do not experience an appreciable increase in e .

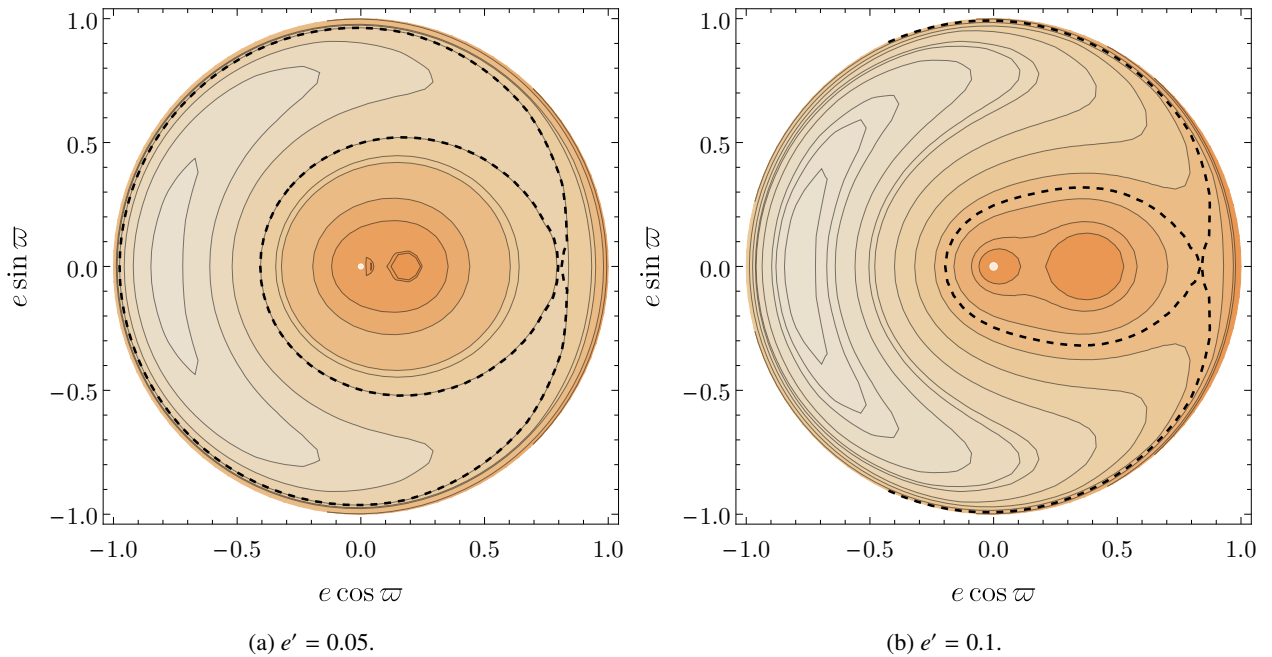


Fig. 4. Same as Fig. 3, but for the 3:1 mean motion resonance with an outer perturber.

where

$$\Phi_0 \equiv \frac{\mathcal{G}m' a^2}{a'^3} \propto \frac{m'}{a}, \quad (5.2)$$

and $\hat{\mathcal{H}}$ is dimensionless. We note that in the above equation, a is really $a_0 = a'/4^{2/3}$ (the value of a in exact Keplerian resonance with the perturber). We assume that the test mass starts with an

initial eccentricity $e_0 \ll 1$ at $\varpi = 0$. Its maximum eccentricity $e_{\max}^{(0)}$ (achieved at $\varpi = \pi$) is determined by

$$\hat{\mathcal{H}}(e_0, 0) - \hat{\mathcal{H}}(e_{\max}^{(0)}, \pi) = 0. \quad (5.3)$$

The superscript “(0)” in $e_{\max}^{(0)}$ indicates that this maximum eccentricity is obtained without any short-range force effect.

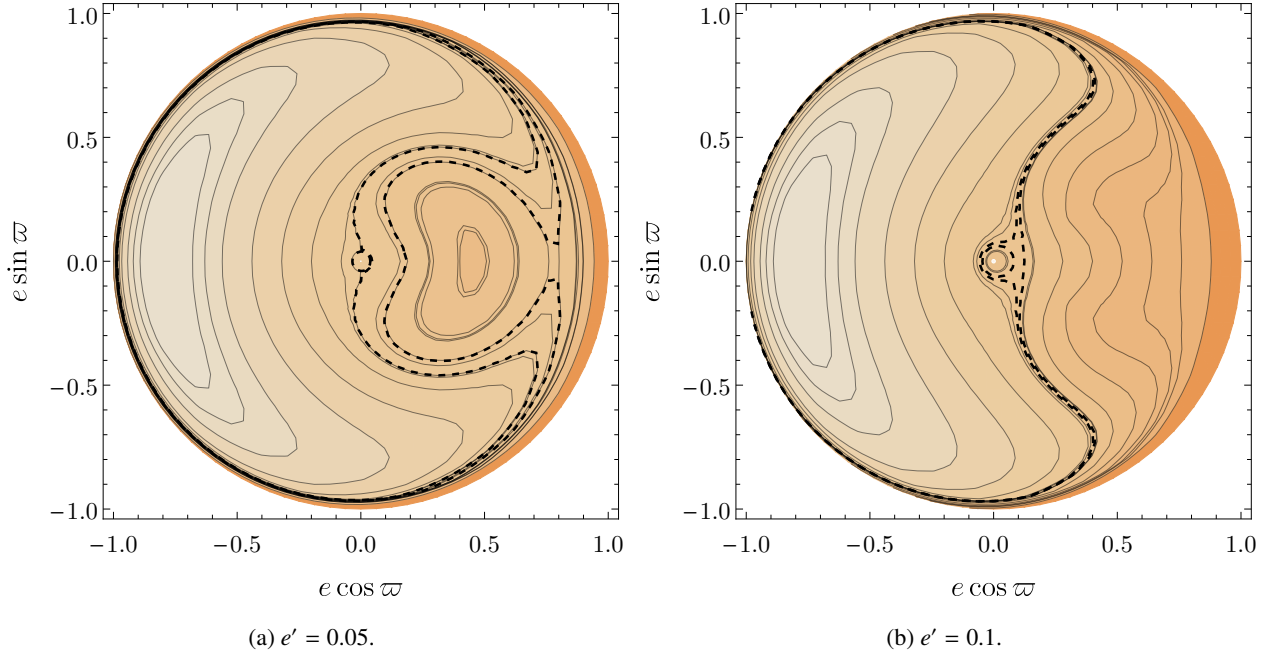


Fig. 5. Same as Fig. 3, but for the 4:1 mean motion resonance with an outer perturber. In contrast to Figs. 3 and 4, orbits with small initial eccentricities can be driven to $e \sim 1$.

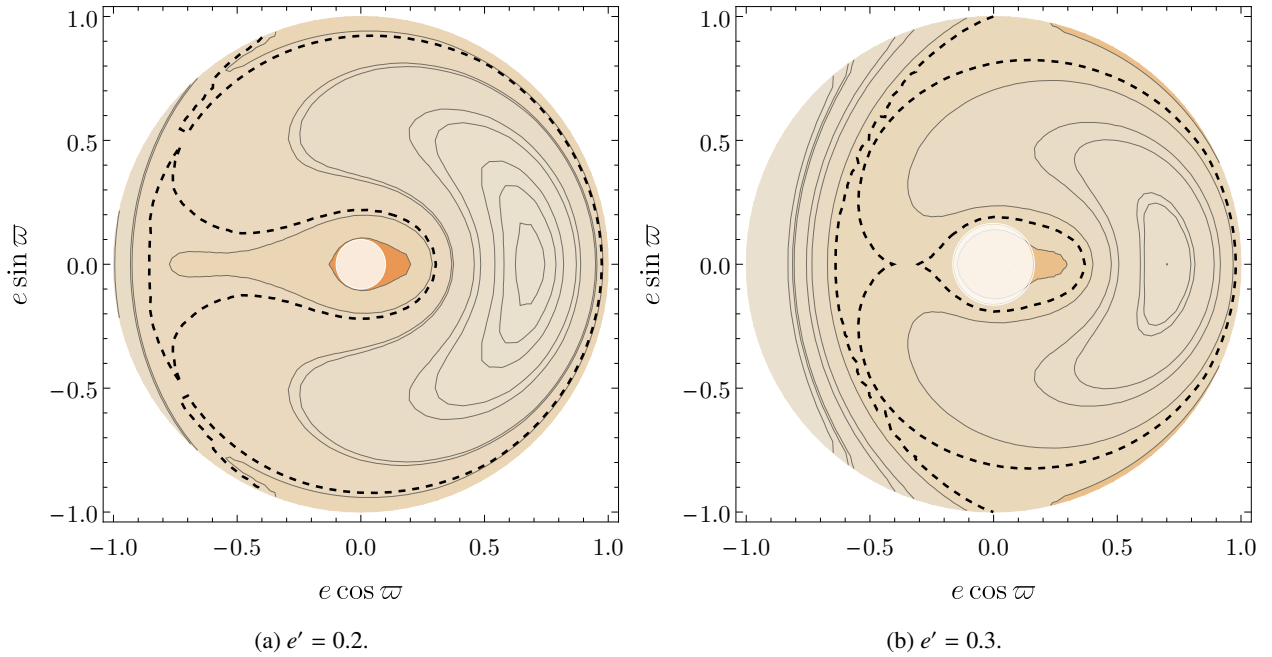


Fig. 6. Level plots of the Hamiltonian $\bar{\mathcal{H}}$ on the $(e \cos \varpi, e \sin \varpi)$ plane for the 2:1 mean motion resonance with an outer perturber with modest eccentricities ($e' = 0.2$ and $e' = 0.3$, both with $\varpi' = 0$). All orbits with initially low eccentricities do not experience a large increase in e .

Now we consider how \mathcal{H}_{GR} affects e_{max} . We write

$$\mathcal{H}_{\text{GR}} = -\frac{\Phi_{\text{GR}}}{\sqrt{1-e^2}}, \quad (5.4)$$

with

$$\Phi_{\text{GR}} \equiv \frac{3\mathcal{G}M_*}{a} \frac{\mathcal{G}M_*}{ac^2}. \quad (5.5)$$

Again, starting with an initial eccentricity $e_0 \ll 1$ at $\varpi = 0$, the maximum eccentricity e_{max} of the test mass (achieved at $\varpi = \pi$)

is estimated by

$$\Phi_0 \hat{\mathcal{H}}(e_0, 0) + \Phi_{\text{GR}} \simeq \Phi_0 \hat{\mathcal{H}}(e_{\text{max}}, \pi) + \frac{\Phi_{\text{GR}}}{\sqrt{1-e_{\text{max}}^2}}. \quad (5.6)$$

Assuming $1 - e_{\text{max}} \ll 1$, Eq. (5.6) becomes

$$\frac{|\mathcal{H}_{\text{GR}}|}{\Phi_0} = \frac{\Phi_{\text{GR}}}{\Phi_0} \frac{1}{\sqrt{1-e_{\text{max}}^2}} \simeq \hat{\mathcal{H}}(e_0, 0) - \hat{\mathcal{H}}(e_{\text{max}}, \pi) =: f. \quad (5.7)$$

This shows that e_{max} depends on various parameters through the ratio $\Phi_{\text{GR}}/\Phi_0 \propto M_*^2/(m'a)$.

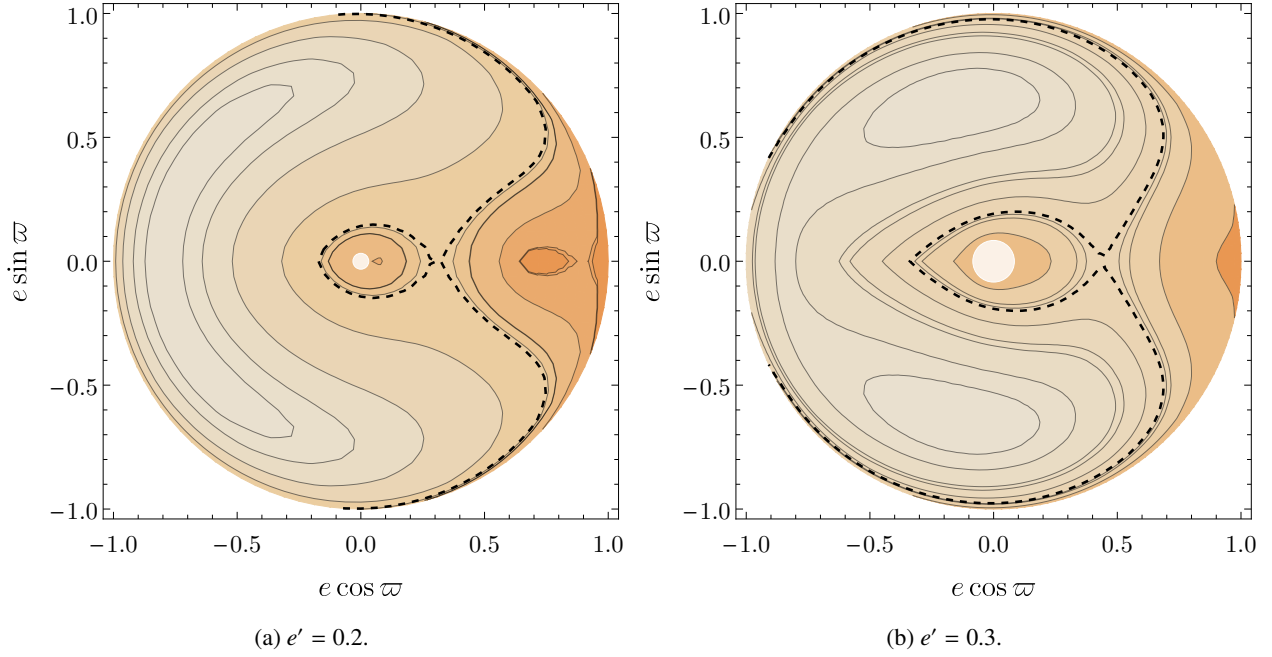


Fig. 7. Same as Fig. 6, but for the 3:1 mean motion resonance with an outer perturber.

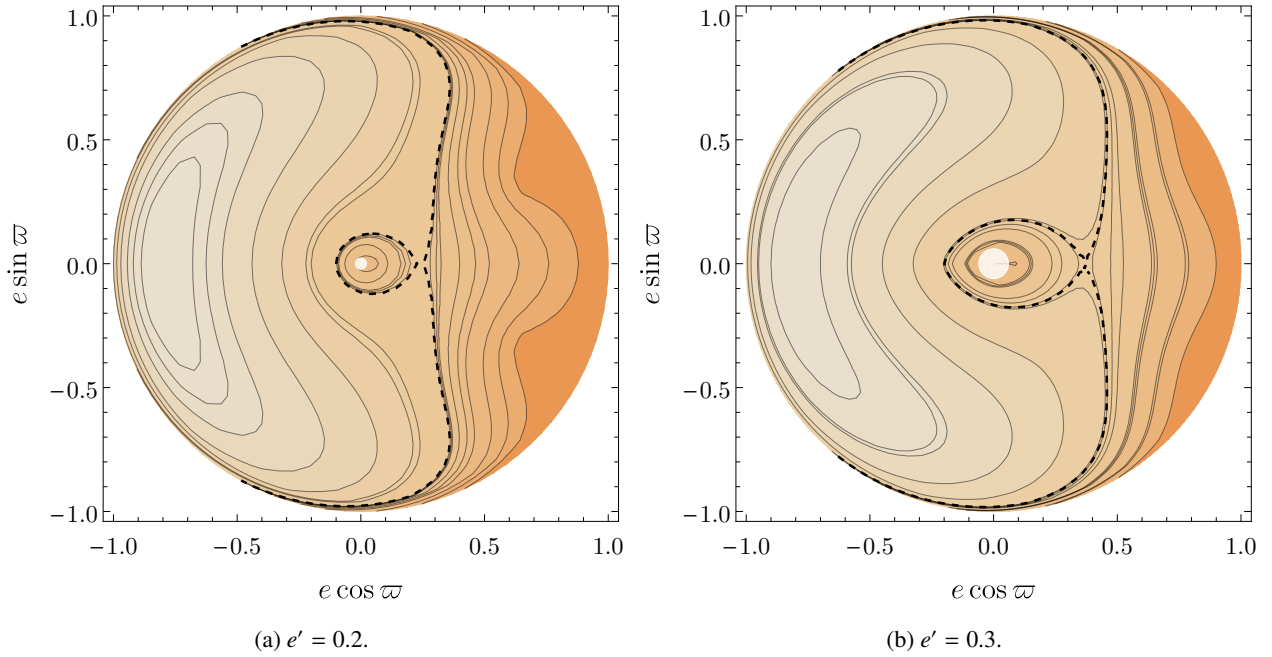


Fig. 8. Same as Fig. 6, but for the 4:1 mean motion resonance with an outer perturber. In contrast to Fig. 5, orbits with initial $e \sim 0$ do not experience extreme eccentricity excitation.

Setting $a(1 - e_{\max}) = R_{\text{crit}}$ in Eq. (5.7), we obtain the critical perturber mass m'_{crit} that allows the test particle to reach a certain pericentre distance R_{crit} :

$$\begin{aligned}
 m'_{\text{crit}} &= \frac{3}{\sqrt{2}} \frac{1}{f} \frac{\mathcal{G} M_*^2}{c^2} \frac{1}{\sqrt{R_*}} a^{-1/2} \left(\frac{a(1 - e_{\max})}{R_*} \right)^{-1/2} \left(\frac{4}{1} \right)^2 \\
 &\simeq 17 M_{\oplus} \left(\frac{f}{0.1} \right)^{-1} \left(\frac{M_*}{M_{\odot}} \right)^2 \left(\frac{a}{\text{AU}} \right)^{-1/2} \left(\frac{R_{\text{crit}}}{R_{\odot}} \right)^{-1/2}.
 \end{aligned} \quad (5.8)$$

It is important to note that f in general depends on e_{\max} and thus is a complicated function of (R_{crit}/a) . However, we can calculate

its numerical value in the case depicted in Figs. 9 and 10, where we obtain $f \sim 0.1$.

6. Conclusions

In this paper, we have revisited the problem of resonant dynamics inside mean motion resonances in the restricted planar three-body problem in order to determine to what extent planetary perturbations can effectively drive small bodies into highly eccentric orbits, and cause them to fall into the star or suffer tidal disruption. While most previous works employed series expansion of the Hamiltonian in powers of the eccentricities or

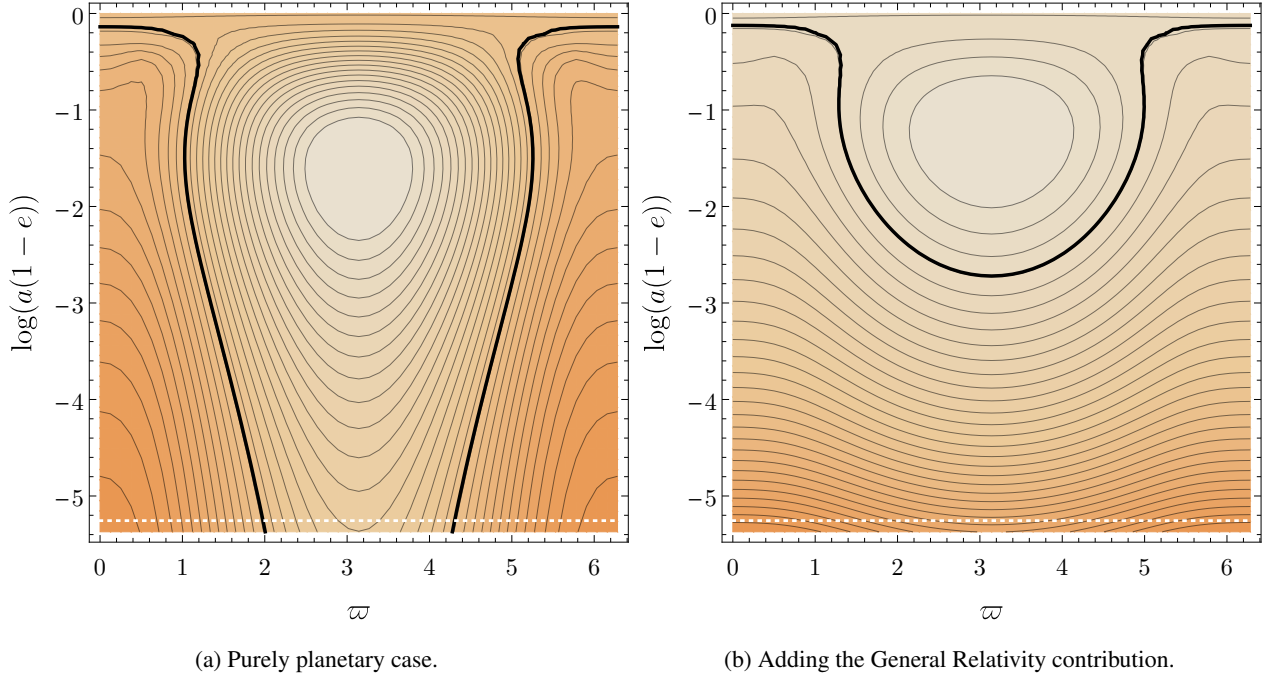


Fig. 9. Level curves of the Hamiltonians $\bar{\mathcal{H}}$ (left panel) and $\bar{\mathcal{H}} + \mathcal{H}_{\text{GR}}$ (right panel) on the $(\varpi, \log a_{\text{peri}})$ plane for a test mass at $a_{\text{res}} = 1$ AU in 4:1 mean motion resonance with an outer perturber with $\mu = 3 \times 10^{-6}$, $\varpi' = 0$ and $e' = 0.1$. The mass of the parent star is set at $M_* = 1 M_{\odot}$. The black solid line experiencing a significant change in a_{peri} indicates the trajectory with the initial conditions $\varpi = 0$ and $e = 0.05$. The lower edge of the plot is at the location of the radius of the star, here taken to be the radius of the Sun (R_{\odot}). The white dotted line indicates the location of the Roche limit, calculated using a density of the test particle of $\rho_{\text{tp}} = 2 \text{ g/cm}^3$. The addition of the General Relativity potential reduces drastically the efficiency of the planetary perturbation in driving the test particle to collide with the star.

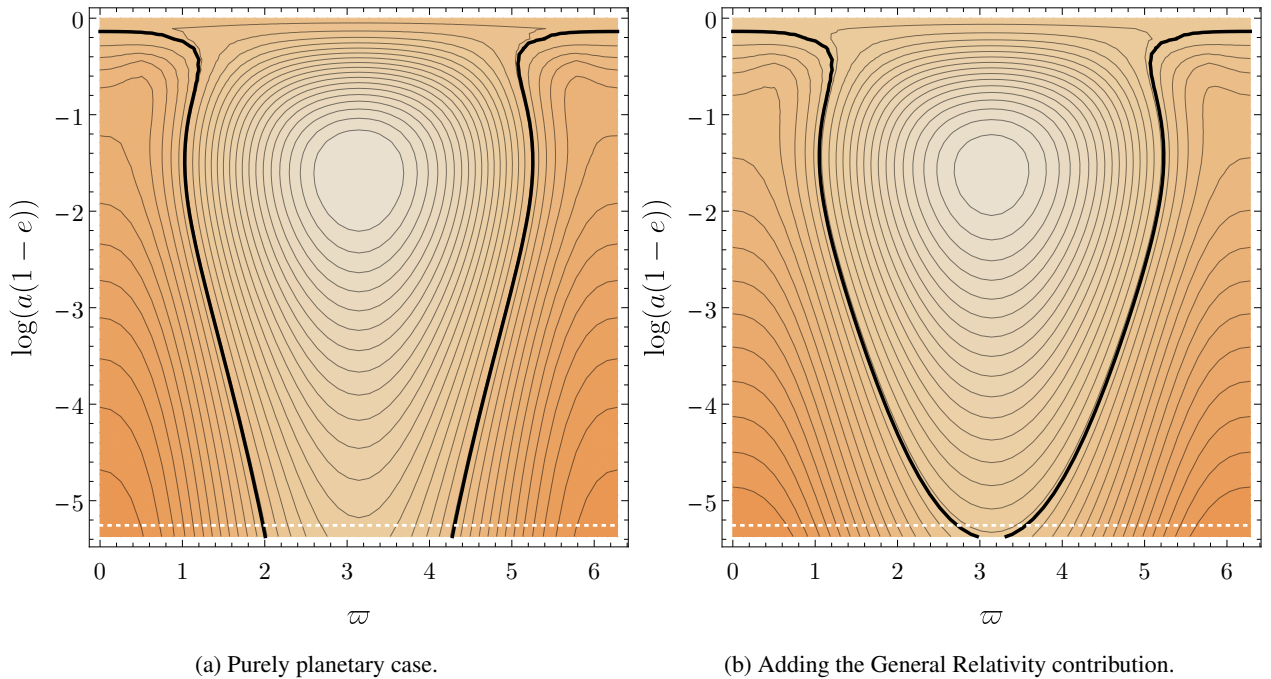


Fig. 10. Same as in Fig. 9, except for $\mu = 5 \times 10^{-5}$. In this case, a test mass starting at $\varpi = 0$ and $e = 0.05$ can fall into the star even considering the General Relativity contribution. The level curves of the purely planetary Hamiltonian do not change with different values of μ : as explained in the text, here μ only plays the role of setting the timescales of the evolution of the test particle, not the evolution itself.

were limited by a first-order development in e' to the case of $e > e'$ and small e' (where e' and e are the eccentricities of the planetary perturber and the test particle, respectively), we do

not perform any expansions, thus making our results valid for a wider range of orbital configurations. We make use of the principle of adiabatic invariance to reduce the two degree of freedom

Hamiltonian (2.10) to the integrable Hamiltonian $\bar{\mathcal{H}}$, which we study in the limit of vanishing amplitude of libration of $k'\lambda' - k\lambda$ in the $k':k = 2:1, 3:1$ and $4:1$ mean motion resonances. We confirm the results of Beust & Morbidelli (1996), and show that for small e' ($\lesssim 0.1$) the $2:1$ and $3:1$ resonances are not able to push test particles in initially nearly circular orbits into star-grazing trajectories (Figs. 3, 4), while the $4:1$ resonance is extremely effective (Fig. 5). Moreover, we find that a higher value of e' ($=0.2-0.3$) does not change this picture for the $2:1$ and $3:1$ resonances (Figs. 6, 7), but makes the $4:1$ resonance less effective by generating a larger stable region of circulation around $e \sim 0$ (Fig. 8). Finally, in the cases where the resonance is strong enough to generate star-grazing objects, we include the General Relativity contribution to the Hamiltonian, which causes a fast precession of the pericentre while keeping the eccentricity constant, thereby suppressing the effectiveness of the planet's perturbation to generate extreme eccentricities (Fig. 9). While the planetary mass only sets the timescales of the secular eccentricity evolution when the General Relativity effect is neglected, we note that it now plays an important dynamical role, as it regulates the relative contribution of the purely Newtonian evolution and the impact of the post-Newtonian term. We then obtain, for a specific choice of semi-major axis and eccentricity of the perturber, an estimate on the minimum planetary mass needed to drive eccentricity growth of the test particle from ~ 0 to ~ 1 . An approximate analytic expression for this critical mass is also obtained. In addition, we make available a Mathematica notebook which implements the calculations outlined in the paper to allow the interested reader to examine the effect of secular dynamics inside mean motion resonances for other applications.

Acknowledgements. G.P. wishes to thank Clément Robert for the valuable advice in improving the readability of the Mathematica code. D.L. acknowledges support by the NASA grants NNX14AG94G and NNX14AP31G, and by a Simons Fellowship in Theoretical Physics from the Simons Foundation. He also thanks the Laboratoire Lagrange OCA for hospitality.

References

- Beaugé, C., Michtchenko, T. A., & Ferraz-Mello, S. 2006, *MNRAS*, **365**, 1160
 Beust, H., & Morbidelli, A. 1996, *Icarus*, **120**, 358
 Beust, H., Lagrange-Henri, A. M., Vidal-Madjar, A., & Ferlet, R. 1989, *A&A*, **223**, 304
 Beust, H., Vidal-Madjar, A., Ferlet, R., & Lagrange-Henri, A. M. 1990, *A&A*, **236**, 202
 Beust, H., Vidal-Madjar, A., Ferlet, R., & Lagrange-Henri, A. M. 1991, *A&A*, **241**, 488
 Bonsor, A., Mustill, A. J., & Wyatt, M. C. 2011, *MNRAS*, **414**, 930
 Debes, J. H., & Sigurdsson, S. 2002, *ApJ*, **572**, 556
 Debes, J. H., Walsh, K. J., & Stark, C. 2012, *ApJ*, **747**, 148
 Marsden, B. G. 1967, *AJ*, **72**, 1170
 Farihi, J. 2016, *New Astron. Rev.*, **71**, 9
 Farinella, P., Froeschle, C., Froeschle, C., et al. 1994, *Nature*, **371**, 315
 Ferlet, R., Vidal-Madjar, A., & Hobbs, L. M. 1987, *A&A*, **185**, 267
 Fontaine, G., & Michaud, G. 1979, *ApJ*, **231**, 826
 Gladman, B. J., Migliorini, F., Morbidelli, A., et al. 1997, *Science*, **277**, 197
 Greaves, J. S., Holland, W. S., Matthews, B. C., et al. 2016, *MNRAS*, **461**, 3910
 Jura, M. 2003, *ApJ*, **584**, L91
 Henrard, J. 1993, *The Adiabatic Invariant in Classical Mechanics, Dynamics Reported* (Springer), 117
 Henrard, J., & Caranicolas, N. D. 1990, *Celest. Mech. Dyn. Astron.*, **47**, 99
 Henrard, J., & Lemaître, A. 1983, *Celest. Mech.*, **30**, 197
 Koester, D., Gänsicke, B. T., & Farihi, J. 2014, *A&A*, **566**, A34
 Krivov, A. V. 1986, *Sov. Astron.*, **30**, 224
 Lagrange, A. M., Ferlet, R., & Vidal-Madjar, A. 1987, *A&A*, **173**, 289
 Lemaître, A. 1984, *Celest. Mech.*, **32**, 109
 Michtchenko, T. A., Beaugé, C., & Ferraz-Mello, S. 2006, *Celest. Mech. Dyn. Astron.*, **94**, 411
 Moons, M., & Morbidelli, A. 1993, *Celest. Mech. Dyn. Astron.*, **57**, 99
 Moons, M., & Morbidelli, A. 1995, *Icarus*, **114**, 33
 Murray, C. D., & Dermott, S. F. 2000, *Solar System Dynamics* (Cambridge, UK: Cambridge University Press)
 Petrovich, C., & Muñoz, D. J. 2017, *ApJ*, **834**, 116
 Sidorenko, V. V. 2006, *Cosmic Res.*, **44**, 440
 Sorelli, C., Grinin, V. P., & Natta, A. 1996, *A&A*, **309**, 155
 Vauclair, G., & Fontaine, G. 1979, *ApJ*, **230**, 563
 Welsh, B. Y., & Montgomery, S. 2013, *PASP*, **125**, 759
 Wisdom, J. 1985, *Icarus*, **63**, 272
 Wisdom, J. 1983, *Icarus*, **56**, 51
 Zuckerman, B., Koester, D., Reid, I. N., & Hüensch, M. 2003, *ApJ*, **596**, 477